JOURNAL OF SPACECRAFT AND ROCKETS
Vol. 43, No. 3, May–June 2006

Two-Dimensional Magnetohydrodynamic Simulation of a Magnetic Sail

Hiroyuki Nishida*
University of Tokyo, Tokyo 113-8656, Japan
Hiroyuki Ogawa,† Ikkoh Funaki,† Kazuhisa Fujita,‡ and Hiroshi Yamakawa§
Japan Aerospace Exploration Agency, Kanagawa 229-8510, Japan
and
Yoshinori Nakayama¶
National Defense Academy, Kanagawa 239-8686, Japan

A magnetic sail (Magsail) is a unique deep-space propulsion system that captures the momentum of the solar wind by a large artificial magnetic field produced around a spacecraft. To clarify the momentum transfer process from the solar wind to the spacecraft, we simulated the interaction between the solar wind and the artificial magnetic field of the Magsail using the magnetohydrodynamic model. The result showed the same plasma flow and magnetic field as those of the magnetic field of the Earth; when the solar wind passes a bow shock, the solar wind is decelerated and deflected because the solar wind cannot penetrate into the magnetic field, which is called the magnetosphere around the spacecraft. The change of the solar-wind momentum resulted in a pressure distribution along the magnetopause, which is the boundary between the solar-wind plasma and the magnetosphere. The pressure on the magnetopause is then transferred to the spacecraft via the Lorentz force between the induced current along the magnetopause and the current along the coil of the spacecraft. The simulation successfully demonstrated that the change of the momentum of the solar wind is transferred to the spacecraft via the Lorentz force, and the drag coefficient of the Magsail was estimated to be 0.9 ± 0.1 when the magnetic dipole is parallel to the solar wind.

Nomenclature

$\boldsymbol{B}$	=	magnetic flux density vector
B_x	=	magnetic flux density in X direction
B_y	=	magnetic flux density in Y direction
B_0	=	normalization magnetic flux density, T
C_d	=	drag coefficient
C_{fx}	=	fast mode wave velocity in X direction, m/s
C_{fy}	=	fast mode wave velocity in Y direction, m/s
C_n	=	courant number
E	=	energy density
$\boldsymbol{F}$	=	thrust vector
F_0	=	normalization thrust, N
$\boldsymbol{I}$	=	unit matrix
$\boldsymbol{J}$	=	current density vector
$\boldsymbol{J}_c$	=	current in the coil of magnetic sail
J_0	=	normalization current density, A
L_c	=	characteristic length, m
p	=	pressure
p_{initial}	=	initial pressure
p_0	=	normalization pressure, Pa
R_E	=	radius of the Earth: 6370 km
$\boldsymbol{r}$	=	position vector
$\boldsymbol{r}_c$	=	position vector of the coil
r_{Li}	=	ion Larmor radius, m
$\boldsymbol{S}$	=	area vector
S_c	=	characteristic area, m^2
T_{sw}	=	temperature of the solar wind
t	=	time
t_0	=	normalization time, s
$\boldsymbol{v}$	=	velocity vector
v_{A0}	=	alfven wave speed
v_{sw}	=	velocity of the solar wind
v_x	=	velocity in X direction
v_y	=	velocity in Y direction
v_0	=	normalization velocity, m/s
γ	=	ratio of specific heat
Δt	=	time step
Δx	=	mesh size in X direction
Δy	=	mesh size in Y direction
μ	=	magnetic moment
μ_0	=	amplitude permeability, H/m
ρ	=	density
ρ_{initial}	=	initial density
ρ_{sw}	=	density of the solar wind
ρ_0	=	normalization density, kg/m^3

Received 24 January 2005; revision received 16 June 2005; accepted for publication 25 July 2005.

*Graduate Student, Department of Aeronautics and Astronautics, 7-3-1 Hongo, Bunkyo-ku.
†Associate Professor, Institute of Space and Astronautical Science, 3-1-1 Yoshinodai, Sagamihara. Member AIAA.
‡Senior Researcher, Institute of Space Technology and Aeronautics, 7-44-1 Jindaiji Higashi-machi, Chofu, Tokyo. Senior Member AIAA.
§Associate Professor, Institute of Space and Astronautical Science, 3-1-1 Yoshinodai, Sagamihara.
¶Lecturer, Department of Aerospace Engineering, 1-10-27 Hashirimizu, Yokosuka. Senior Member AIAA.

I. Introduction

THE outer solar system is still vastly unexplored because deep-space exploration takes a very long time. It is difficult for traditional propulsion systems to perform such deep-space missions in a short period; hence a new propulsion system with high thrust as well as high efficiency is required to shorten mission time drastically. A promising candidate for such a short-term deep-space mission is a magnetic sail.

The magnetic sail produces a large magnetic field around a spacecraft and generates thrust through the interaction between the solar wind and the magnetic field (Fig. 1). The solar wind is a high-speed plasma flow from the sun in the interplanetary space. To generate enough large thrust to propel the spacecraft, a large-scale magnetic field has to be created by expanding a superconducting coil of several

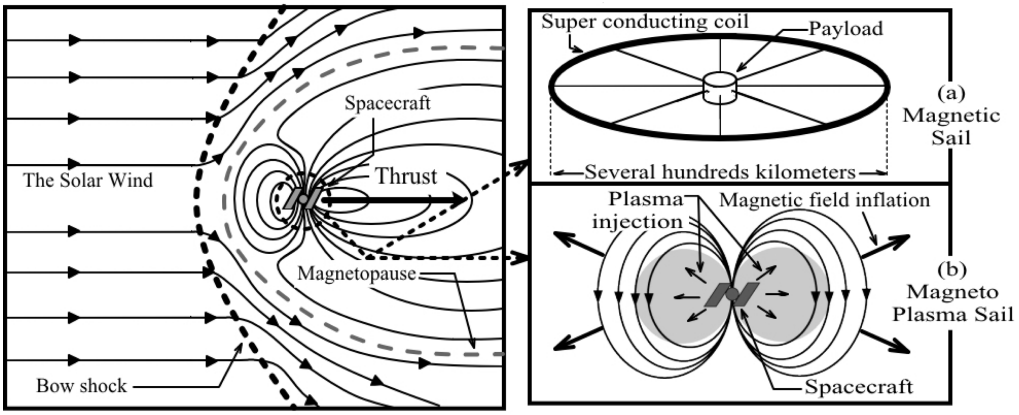

Fig. 1 Propulsion systems making use of the solar wind.

hundred kilometers in diameter[1] (Fig. 1a). It is, however, difficult to deploy such a large structure. To overcome this difficulty, a new method was proposed by Winglee et al.[2] The method uses plasma injection from the spacecraft to inflate the magnetic field (Fig. 1b). The method is originally called as M2P2 (minimagnetospheric plasma propulsion), which is sometimes denoted as a plasma sail or a magneto plasma sail (MPS). The magnetic sail with plasma jet does not need any huge structures, and therefore it is more realistic if it is feasible. However, whether MPS is feasible or not is still under discussion.[3–9]

The magnetic sail and its derivatives generate thrust by the interaction between the solar wind and the magnetic field of the spacecraft. To clarify the thrust-generation process and performance of these propulsion systems, some numerical simulations have been conducted by hybrid models[6–8] and particle-in-cell[9] models for the case that the magnetic field of the spacecraft interacts with the solar wind in kinetic scale of ions. If the ion Larmor radius exceeds the size of the MPS magnetic field, only small interactions, hence small thrust, are expected.[1–6] Therefore the spacecraft needs to produce a large-scale magnetic field, which interacts with the solar wind in magnetohydrodynamic (MHD) scale in order to achieve high performance.

When the solar wind interacts with the magnetic field of the spacecraft in the MHD scale, a bow shock is formed, and the solar wind is decelerated and deflected when passing the bow shock. In this case the magnetic field is pushed downstream by the solar wind, and the magnetosphere is formed around the spacecraft. The solar wind flows around the magnetosphere because the flow cannot enter into it if we assume the ideal MHD flow without any diffusive effects. If the magnetosphere were a solid object, the pressure distribution of the solar wind on the boundary of the magnetosphere would directly push the magnetosphere (spacecraft). However, the thrust-generation process of the magnetic sail is more complicated because the force cannot be directly exerted on the spacecraft. It is expected that the momentum change of the solar wind to the spacecraft transfers through some kind of electromagnetic interaction. Although Zubrin and Andrews evaluated the performance of the magnetic sail,[1] they assumed a drag coefficient of unity and estimated the size of the magnetosphere by simple pressure balance between the magnetic and the dynamic pressures of the solar wind. Zubrin and Andrews did not simulate the interaction between the solar wind and the magnetic field based on the self-consistent MHD model. In contrast, Winglee et al. evaluated the whole flowfield of M2P2[2]; they evaluated the change of the solar-wind momentum. However, they did not discuss how the momentum change of the solar wind transfers to the spacecraft.

In this research, we simulate the interaction between the solar wind and the magnetic field based on the ideal MHD model to identify action and reaction forces and their balance (i.e., a check that the simulation includes all action-reaction pairs). Then, the thrust is evaluated for various magnetic field configurations described.

II. Simulation Model

A. Basic Equations and Numerical Method

We adopt one-fluid ideal MHD equations to simulate the interaction between the solar wind and the magnetic field. Normalized ideal MHD equations are

$$\frac{\partial \rho}{\partial t} + \nabla \cdot (\rho \boldsymbol{v}) = 0 \tag{1}$$

$$\frac{\partial \rho \boldsymbol{v}}{\partial t} + \nabla \cdot (\rho \boldsymbol{v}\boldsymbol{v} + p\boldsymbol{I}) = \boldsymbol{J} \times \boldsymbol{B} \tag{2}$$

$$\frac{\partial \boldsymbol{B}}{\partial t} - \nabla \times (\boldsymbol{v} \times \boldsymbol{B}) = 0 \tag{3}$$

$$\frac{\partial E}{\partial t} + \nabla \cdot \left[\left(E + p + \frac{B^2}{2} \right) \boldsymbol{v} - \boldsymbol{B}(\boldsymbol{B} \cdot \boldsymbol{v}) \right] = 0 \tag{4}$$

$$\boldsymbol{J} = \nabla \times \boldsymbol{B} \tag{5}$$

where E is energy density:

$$E = \tfrac{1}{2}\rho v^2 + p/(\gamma - 1) + B^2/2 \tag{6}$$

The normalization quantities in the basic equations are $L_0 =$ the coil radius of magnetic sail, $B_0 = 2 \times 10^{-8}$ T, and $\rho_0 = m_i \times 10^6\,\mathrm{kg/m^3}$, where m_i is the mass of proton; 1.672×10^{-27} kg. The other normalization quantities are defined by these units: $v_0 = B_0/(\mu_0\rho_0)^{1/2}$, $t_0 = L_0/v_0$, $p_0 = \rho v_0^2$, and $J_0 = B_0/(L_0\mu_0)$. In addition, force vector $\boldsymbol{F}$ is normalized by $F_0 = \rho_0 v_0^2 \cdot L_0^2$.

In this study, these ideal MHD equations are solved numerically by the flux-corrected-transport (FCT) scheme.[10,11]

To confirm reliability of our FCT code, the one-dimensional MHD equations with the following Riemann data are solved. The Riemann problem is as follows:

$$(\rho, v_x, v_y, B_x, B_y, p) = \begin{cases} (1.000, 0, 0, 0.75, +1.0, 1.0) & X \le 0 \\ (0.125, 0, 0, 0.75, -1.0, 0.1) & X > 0 \end{cases} \tag{7}$$

with $\gamma = 2$. This problem has been suggested by Brio and Wu[12] and is commonly used to test numerical schemes for ideal MHD. Figure 2 shows the distributions of the density, the velocity components, the magnetic field components, and the pressure by our FCT code. The numerical solutions at $t = 80.0$ are obtained for 800 grid points with $\Delta x = 1.0$ and $\Delta t = 0.025$. Note that in Fig. 2, a solution obtained for 20,000 grid points with $\Delta x = 0.04$ and $\Delta t = 0.001$ is also shown as an exact solution with dashed line. A fast rarefaction wave (FR1) and a slow compound wave (SM) propagate to the left from the origin. A contact discontinuity (C), a slow shock (SS), and a fast rarefaction wave (FR2) propagate to the right. There is an undershoot at the back of FR2 and at C. Numerical oscillations arise between C and SM and between SS and FR2. On the other hand, the discontinuities

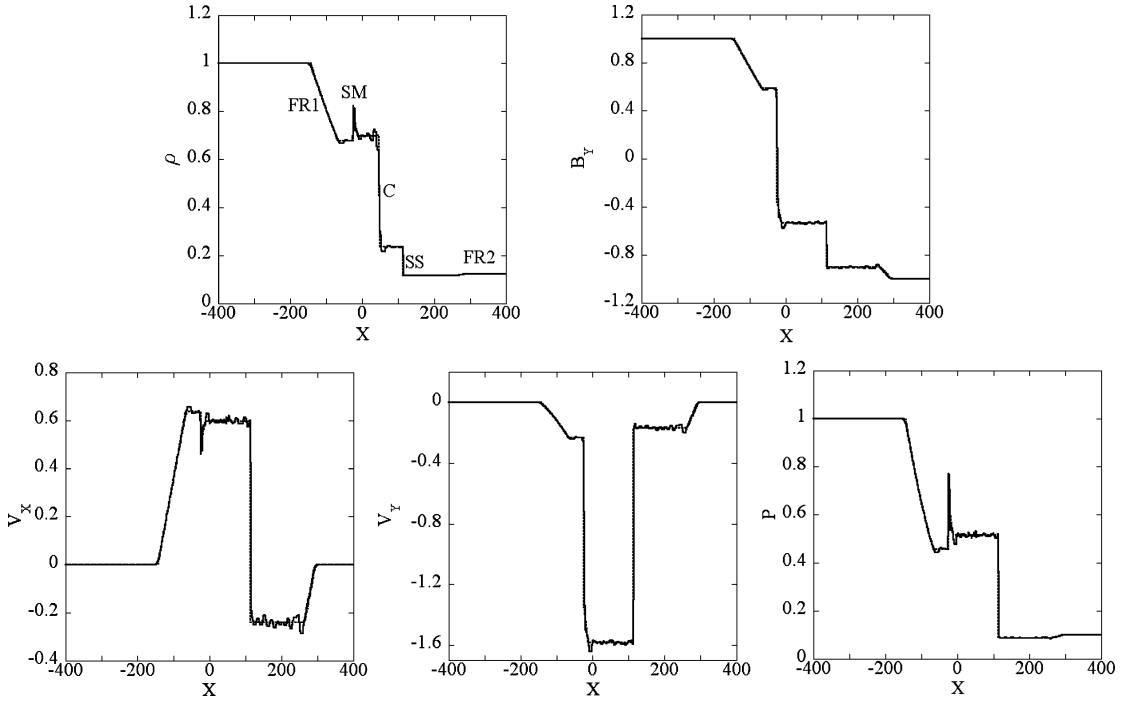

Fig. 2 Riemann problem of Brio and Wu with 800 grid points at $t = 80.0$ by FCT code.

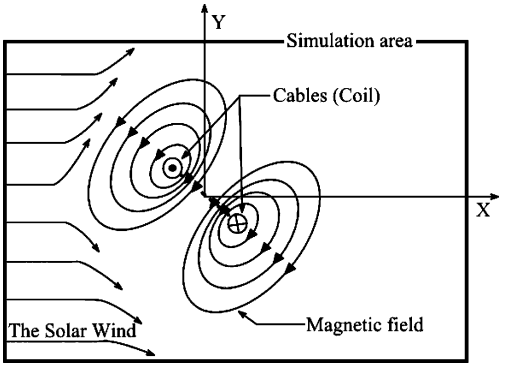

Fig. 3 Simulation box.

are resolved sharply. The results are in good agreement with those obtained by Brio and Wu.[12] Therefore, reliability of our FCT code was confirmed.

B. Computational Conditions

In this study, the interaction between the solar wind and the magnetic field is simulated in two-dimensional space. The simulation box is defined to be a rectangular coordinate system as shown in Fig. 3, where the X axis is along the sun–magnetic sail line.

Two rigid cables with an electric current flowing in the direction perpendicular to the X–Y plane are located so that the middle point between them is the origin. The cables correspond to the coil of the magnetic sail. The solar wind is introduced through the boundary of the simulation box at the beginning of the simulation and flows into the box in the X direction. The simulation was terminated when a steady state was achieved. The simulation area is defined over $-5 \le X \le 7$, $-6 \le Y \le 6$ in units of the radius of the coil L_0. This simulation area is divided into Cartesian grid systems.

The initial magnetic field is produced by the superposition of the first magnetic field in Fig. 3 with a second symmetric magnetic field placed past the sunward boundary outside the simulation box. Because of this second magnetic field, magnetic field lines perpendicular to the sunward boundary are removed[13] at that boundary. The "original" magnetic field is produced by the electric currents in the two cables. This initial magnetic field is filled with static plasma of a constant kinetic pressure ($p_{\text{initial}} = 0.1\,p_0$). The initial plasma density distribution is set so that the Alfven wave velocity is constant ($v_{A0} = 700$ km/s) in the area where the magnetic field is strong and the initial plasma density is set to be constant in the area where the field is weak:

$$\begin{cases} \rho_{\text{initial}} = B^2 \big/ v_{A0}^2 & \text{where} \quad \rho_{\text{initial}} > 0.01\rho_{\text{sw}} \\ \rho_{\text{initial}} = 0.01\rho_{\text{sw}} & \text{where} \quad \rho_{\text{initial}} \le 0.01\rho_{\text{sw}} \end{cases} \tag{8}$$

The boundary conditions in the Y direction and at the downstream boundary are treated by linear extrapolation of the fluid and magnetic quantities, so that the solar wind leaves the simulation box easily. At the sunward boundary, quantities are set by typical solar-wind parameters:

$$\rho_{\text{sw}} = 5.0\left(5\,m_i \times 10^6\ \text{kg/m}^3\right), \qquad \boldsymbol{B}_{\text{sw}} = 0$$

$$P_{\text{sw}} = 8.68 \times 10^{-2}\ (T_{\text{sw}} = 20\,\text{eV}), \qquad v_{\text{sw}} = 0.917(400\,\text{km/s})$$

The boundary conditions at the coil are set by fixing all quantities at their initial values. In this simulation, the boundary of the coil is set at $0.2\,L_0$ away from the center of each cable.

Setting of the time step Δt is determined based on the Courant number C_n:

$$\Delta t = C_n \text{MIN}[\Delta x/(|v_x| + C_{fx}),\ \Delta y/(|v_y| + C_{fy})] \tag{9}$$

where

$$C_{fx}^2 = \tfrac{1}{2}\left\{[(\gamma p + B^2)/\rho] + \sqrt{[(\gamma p + B^2)/\rho]^2 - 4(\gamma p/\rho)\left[B_x^2/\rho\right]}\right\} \tag{10}$$

$$C_{fy}^2 = \tfrac{1}{2}\left\{[(\gamma p + B^2)/\rho] + \sqrt{[(\gamma p + B^2)/\rho]^2 - 4(\gamma p/\rho)\left[B_y^2/\rho\right]}\right\} \tag{11}$$

$$B^2 = B_x^2 + B_y^2 \tag{12}$$

Here MIN operates over the entire simulation area. The FCT scheme is stable when the Courant number is smaller than 0.5, and the Courant number in this simulation is set to be 0.49.

III. Results and Discussion

A. Flowfield Around the Magnetic Sail

In the simulation, the electric current through the coil ($|\boldsymbol{J}_c|$) is set to be 1.2×10^{12}; here $|\boldsymbol{J}_c|$ is the normalized value. The interactions between the solar wind and the magnetic field were simulated in various coil tilt angles, and the forces were calculated in each case. Here the coil tilt angle is defined between the solar-wind flow direction and the coil.

Figure 4 shows the simulation result of the flowfield in the case where the coil tilt angle is 0 deg. Note that all quantities indicated in this figure are normalized. The pressure contours and the streamlines of the solar wind are in Fig. 4a, the induced current distribution is in Fig. 4b, and the magnetic field lines are in Fig. 4c. It can be observed in Fig. 4a that a bow shock is formed in front of the coil and that the magnetosphere, which is the area of the spacecraft's magnetic field, is formed around the coil. The solar wind flows around the magnetosphere without entering into it. The magnetic field is moved and stretched toward the downstream region of the solar wind, and the induced current flows on the boundary and inside of the magnetosphere perpendicular to the X-Y plane (Figs. 4b and 4c). Figure 5 shows the simulation result of the flowfields of the cases of various coil tilt angles. Figures 5a–5c show the pressure contours and streamlines of the case where coil tilt angles are 0, 45, and 90 deg, respectively. The size of the magnetosphere reduces with an increase in the coil tilt angle, and the shapes of the magnetosphere in front of the coil in the cases that the coil tilt angle are 45 and 90 deg are totally different from the shape of the case where the coil tilt angle is 0 deg. The solar wind enters into the area in between two cables; this area is called the cusp. Pressure in the cusp is higher because the cusp captures the solar wind.

B. Evaluation of Thrust

It can be thought that the magnetic sail generates thrust by receiving the momentum of the solar wind through electromagnetic interaction. Three forces described next are calculated to verify the balance of forces involved in the system and to estimate thrust on the magnetic sail accurately.

1. *Momentum Change of the Solar Wind*

The force acting on the solar wind $\boldsymbol{F}_1$ is calculated by integrating all momentum that flows into and out of the simulation area (Fig. 6):

$$\boldsymbol{F}_1 = \oint (\rho \boldsymbol{v}\boldsymbol{v} + p\boldsymbol{I})\, \mathrm{d}\boldsymbol{S} \tag{13}$$

where this integration operates over the entire boundary of the simulation area.

2. *Pressure Balance on the Magnetopause*

Because the solar wind flows around the magnetosphere without entering into the magnetosphere, the pressure distribution is produced on the magnetopause. The force $\boldsymbol{F}_2$ is calculated by

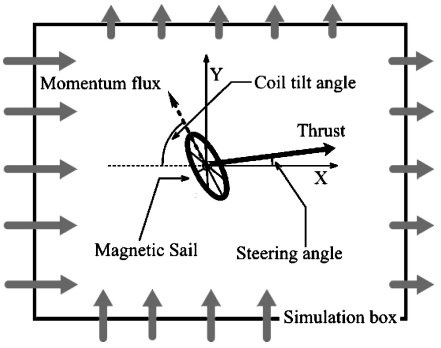

Fig. 6 Momentum change of the solar wind.

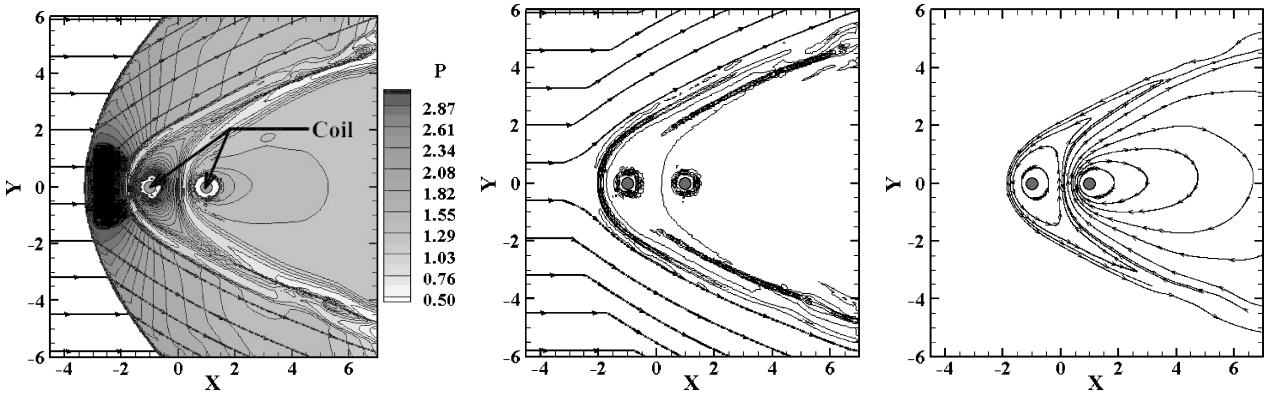

a) Pressure contours and streamlines **b) Currents contours and streamlines** **c) Magnetic field lines**

Fig. 4 Flowfield around the magnetic sail (coil tilt angle = 0 deg).

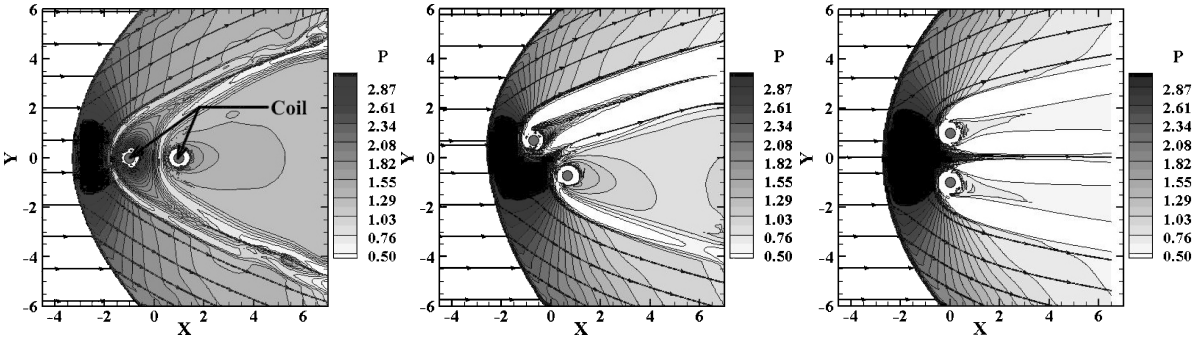

a) Coil tilt angle = 0 deg **b) Coil tilt angle = 45 deg** **c) Coil tilt angle = 90 deg**

Fig. 5 Flowfield dependency on the coil tilt angle (pressure contours and streamlines).

integrating pressure along the line of the magnetopause:

$$\boldsymbol{F}_2 = \oint p \, \mathrm{d}\boldsymbol{S} \tag{14}$$

3. Lorentz Force Between the Induced Currents and the Magnetic Sail

The third force is the Lorentz force. As the simulation result shows, induced currents flow in the magnetosphere. The Lorentz force between the induced currents and the current through the coil of the magnetic sail works as thrust (Fig. 7). The Lorentz force on the coil $\boldsymbol{F}_3$ is

$$\boldsymbol{F}_3 = \int \left[\frac{\boldsymbol{J}_c \cdot \boldsymbol{J}(\boldsymbol{r})}{2\pi |\boldsymbol{r}_c - \boldsymbol{r}|} \frac{(\boldsymbol{r}_c - \boldsymbol{r})}{|\boldsymbol{r}_c - \boldsymbol{r}|} \right] \mathrm{d}S \tag{15}$$

where this integration operates over the entire simulation area.

Figure 8 shows the relation between the coil tilt angle and the forces calculated by three approaches. Here the forces are the normalized forces per unit thickness in a direction perpendicular to the X–Y plane because two-dimensional space is assumed in this simulation. In Fig. 9, to calculate the force based on the pressure distribution on the magnetopause, the cavity of the magnetic field

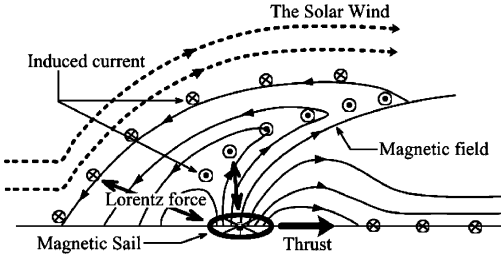

Fig. 7 Lorentz force between the induced current and magnetic sail.

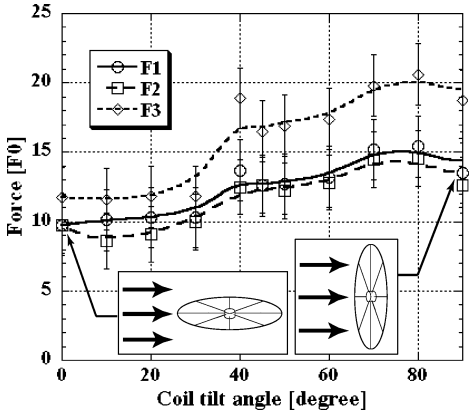

Fig. 8 Relation between the coil tilt angle and thrust.

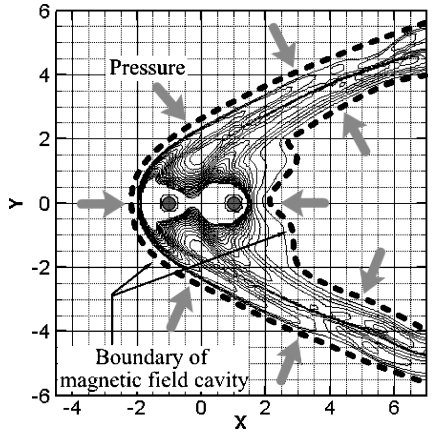

Fig. 9 Cavity of magnetic field.

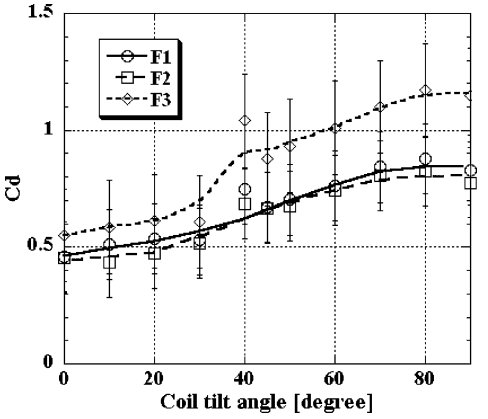

Fig. 10 Relation between the coil tilt angle and drag coefficient.

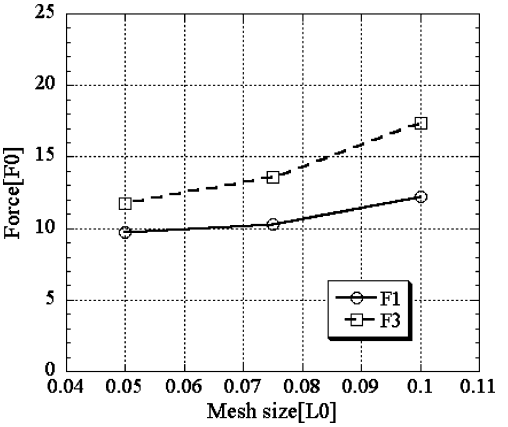

Fig. 11 Force dependence on the mesh size.

is defined for $|B|^2 > 0.4$. Figure 9 shows contours of magnetic field intensity $|B|^2$ and the cavity of the magnetic field with dashed lines in the case that the coil tilt angle is 0 deg. A high-pressure area, called the plasma sheet, exists behind the coil, and so the cavity of the magnetic field is also pressed by the plasma sheet (shown in Fig. 9). For the other cases of the coil tilt angles, the cavity is defined in a similar way. Figure 10 shows the relation between the coil tilt angle and the drag coefficient. The drag coefficient is defined:

$$C_d = D \Big/ \tfrac{1}{2} \rho_{\mathrm{sw}} v_{\mathrm{sw}}^2 S_c \tag{16}$$

Here S_c, the characteristic area, is determined to be the cross-section area of the outside boundary of the magnetic field cavity at $X = 7.0$ (shown in Fig. 9) for the respective coil tilt angle. As shown in Figs. 8 and Fig. 10, forces calculated by three approaches are in same trend; thrusts basically become larger as the coil tilt angle becomes larger, and then the drag coefficient gets up to 0.7–0.9 when the coil tilt angle is 80–90 deg. The cause of increasing drag coefficients with the coil tilt angle is that the cusp captures the solar wind when the coil tilt angle is large. Although the forces at 90 deg are slightly less than those at 80 deg, the drag coefficient is maximal at 90 deg. This is because the magnetic field cavity becomes reduced in size with an increase in the coil tilt angle; the characteristic area changes in response to each coil tilt angle.

Although each force in Fig. 8 is of the same order, F3 is larger than F1 and F2. It can be thought that the differences are caused by the space resolution of grids for calculation. To analyze the dependence on the mesh size, we simulated with three different mesh sizes in the case where the coil tilt angle is 0 deg. Figure 11 shows the relation between the evaluated forces ($F1$ and $F3$) and mesh sizes. As shown in Fig. 11, $|F3 - F1|$ decreases as the mesh size becomes small. Therefore if the mesh size is small enough, $|F3 - F1|$ will reduces to zero. For that reason, the error bars in Figs. 8 and 10 were estimated based on the space resolution of grids.

Table 1 Scale of magnetic sail

Radius of the coil, km	Radius of magnetosphere, km	Current in the coil, kA	Thrust, mN/m	r_{Li}/L_c	MHD validity
10	40	1.5	0.05	1.25	×
20	80	3	0.1	0.625	△
40	160	6	0.2	0.312	△
100	400	15	0.5	0.125	○
200	800	30	1	0.0625	○

Next, we measured the effect of fixing all quantities at their initial values in the vicinity of the coil. There are some possibilities that plasma erupts from, or is absorbed by, the boundary at the coil. Errors in conservation of mass are analyzed in order to estimate the effect of the boundary at the coil. As the result of the analysis, it is found that only small amounts of plasma are absorbed at the boundary of the coil: the amount of absorbed plasma is less than 1% of total mass of the solar wind, which flows into the simulation box. Therefore the effects on the evaluated forces are negligible.

From the just-mentioned results, the three forces were verified to be the same, hence, Newton's third law of motion applied to the system within the accuracy of the simulation. So the momentum transfer process was clarified as follows. First, the solar wind is decelerated and deflected by the presence of the magnetic field around the spacecraft. Second, the solar-wind's dynamic pressure deforms the spacecraft's magnetic field into the magnetosphere. Third, the solar wind flows around the magnetosphere and forms pressure distribution on the magnetopause. Fourth, the induced currents flow on the magnetopause, and the Lorentz force between the currents on the magnetopause and the magnetic field created by those induced currents balances with the pressure distribution. Finally, the Lorentz force between the magnetic fields by the induced currents and the current of the spacecraft's coil turns into thrust.

C. Scale of Magnetic Sail

In this subsection, we discuss the real scale of the magnetic sail treated in this study. Table 1 shows the radius of the magnetosphere, the electric current in the coil, and the thrust for the cases where the radii of the coil are 10, 20, 40, 100, and 200 km. Note, however, that the thrusts shown in Table 1 are thrust per unit thickness of the field in the direction perpendicular to the X–Y plane.

The interaction between the plasma flow and the magnetic field is classified by the ratio of the ion Larmor radius and characteristic length r_{Li}/L_c. In the case of $r_{\mathrm{Li}}/L_c \ll 1$, the process is a MHD scale. In contrast, in the case of $r_{\mathrm{Li}}/L_c \geq 1$ the process is not dominated by MHD, but by the kinetic scale of the ions. In Table 1, the parameters r_{Li}/L_c are listed, where L_c is defined to be diameter of the magnetosphere at $X = 7.0$. As can be seen, the simulation in this study is valid in the case that the radius of the coil is larger than 100 km.

IV. Summary

In this study, the interaction between the solar wind and the magnetic field of magnetic sail was simulated using the ideal MHD equations by the flux-corrected-transport scheme, and three kinds of forces were evaluated: 1) momentum change of the solar wind, 2) the pressure distribution on the boundary of the spacecraft's magnetic field cavity, and 3) the Lorentz force between the induced current and the currents through the coil. These forces were evaluated and analyzed for various coil tilt angles, and then the balance of these three forces was verified; therefore, the process of the solar-wind momentum transfer to the spacecraft was clarified. The process is as follows: first, the solar wind is decelerated and deflected by the magnetic field of the spacecraft. Second, the magnetic field is stretched downstream by the solar wind and forms the magnetosphere around the spacecraft. Third, the solar wind flows around the magnetosphere and produces pressure distribution on the magnetopause. In the magnetopause, induced currents flow, and the Lorentz force between the currents on the magnetopause and the magnetic field produced by the induced currents balances with the pressure distribution. Finally, the Lorentz force between the magnetic field produced by the induced currents and the currents of the coil of the spacecraft corresponds to thrust. The maximum drag coefficient of the magnetic sail was estimated to be 0.9 ± 0.1 when the coil tilt angles is 90 deg.

This study solved a couple of the important problems related to the magnetic sail. This study should be of considerable aid in researching the magneto plasma sail, which is a more complicated but more realistic propulsion system.

Acknowledgments

We gratefully acknowledge the support and advice of Yoshifumi Inatani, the magneto-plasma-sail research group members, and solar-terrestrial physics group members at the Institute of Space and Astronautical Science.

References

[1]Zubrin, R., and Andrews, D., "Magnetic Sails and Interplanetary Travel," *Journal of Spacecraft and Rockets*, Vol. 28, No. 2, 1991, pp. 197–203.

[2]Winglee, R. M., Slough, J., Ziemba, T., and Goodson, A., "Mini-Magnetospheric Plasma Propulsion: Tapping the Energy of the Solar Wind for Spacecraft Propulsion," *Journal of Geophysical Research*, Vol. 105, No. 21, 2000, pp. 67–77.

[3]Asahi, R., Funaki, I., Fujita, K., Yamakawa, H., Ogawa, H., Nonaka, S., Sawai, S., Nishida, H., Nakayama, Y., and Otsu, H., "Numerical Study on Thrust Production Mechanism of a Magneto Plasma Sail," AIAA Paper 2004-3502, July 2004.

[4]Winglee, R. M., Euripides, P., Ziemba, T., Slough, J., and Giersch, L., "Simulation of Mini-Magnetospheric Plasma Propulsion (M2P2) Interaction with an Eternal Plasma Wind," AIAA Paper 2003-5224, July 2003.

[5]Yamakawa, H., "Guidance Strategy for Radially Accelerated Trajectories," *Journal of Spacecraft and Rockets*, Vol. 42, No. 4, 2005, pp. 677–683.

[6]Khazanov, G., Delamere, P., and Kabin, K., "Fundamentals of The Plasma Sail Concept: MHD and Kinetic Studies," AIAA Paper 2003-5225, July 2003.

[7]Omidi, N., and Karimabadi, H., "Kinetic Simulation/Modeling of Plasma Sail," AIAA Paper 2003-5226, July 2003.

[8]Saha, S., Singh, N., Craven, P., Gallagher, D., and Jones, J., "Development of 3D Hybrid Code and Its Application to M2P2," *Space Technology and Applications International Forum-STAIF*, edited by M. S. El-Genk, American Inst. of Physics, New York, 2001, p. 441.

[9]Fujita, K., Funaki, I., Ogawa, H., and Yamakawa, H., "Numerical Investigation of Acceleration Processes in MagnetoPlasmaSail," International Symposium on Space Technology and Science, Paper 2004-o-3-07v, June 2004.

[10]Devore, C. R., "Flux-Corrected Transport Algorithms for Two-Dimensional Compressible Magnetohydrodynamics," Naval Research Lab., Memorandum Rept. 6544, Washington, DC, Sept. 1989.

[11]Devore, C. R., "An Improved Limiter for Multidimensional Flux-Corrected Transport," Naval Research Lab., Memorandum Rept. 6440-98-8300, Washington, DC, Dec. 1998.

[12]Brio, M., and Wu, C. C., "An Upwind Differencing Scheme for the Equations of Ideal Magnetohydrodynamics," *Journal of Computational Physics*, Vol. 75, April 1988, pp. 400–422.

[13]Watanabe, K., and Sato, T., "Global Simulation of the Solar Wind-Magnetosphere Interaction: The Importance of Its Numerical Validity," *Journal of Geophysical Research*, Vol. 95, No. A1, 1990, pp. 75–88.

A. Ketsdever
Associate Editor